J. Plasma Phys. (2020), *vol*. 86, 905860508
Published by Cambridge University Press

doi:10.1017/S0022377820001130

Comparative study of the surface potential of magnetic and non-magnetic spherical objects in a magnetized radio-frequency discharge

Mangilal Choudhary[1],†, **Roman Bergert**[1], **Slobodan Mitic**[1] and **Markus H. Thoma**[1]

[1]I. Physikalisches Institut, Justus–Liebig Universität Giessen, Henrich–Buff–Ring 16, D 35392 Giessen, Germany

(Received 2 January 2020; revised 20 August 2020; accepted 2 September 2020)

We report measurements of the time-averaged surface floating potential of magnetic and non-magnetic spherical probes (or large dust particles) immersed in a magnetized capacitively coupled discharge. In this study, the size of the spherical probes is taken greater than the Debye length. The surface potential of a spherical probe first increases, i.e. becomes more negative at low magnetic field ($B < 0.05$ T), attains a maximum value and decreases with further increase of the magnetic field strength ($B > 0.05$ T). The rate of change of the surface potential in the presence of a B-field mainly depends on the background plasma and types of material of the objects. The results show that the surface potential of the magnetic sphere is higher (more negative) compared with the non-magnetic spherical probe. Hence, the smaller magnetic sphere collects more negative charges on its surface than a bigger non-magnetic sphere in a magnetized plasma. The different sized spherical probes have nearly the same surface potential above a threshold magnetic field ($B > 0.03$ T), implying a smaller role of size dependence on the surface potential of spherical objects. The variation of the surface potential of the spherical probes is understood on the basis of a modification of the collection currents to their surface due to charge confinement and cross-field diffusion in the presence of an external magnetic field.

Key words: electric discharges, dusty plasmas, plasma devices

1. Introduction

A spherical object or dust grain attains an equilibrium potential (or floating potential) when it is immersed in a plasma. At the floating potential, it draws a net zero current, i.e. the net flux of electrons and ions to the surface of the spherical object is zero. In low-temperature plasmas, where the electron temperature is much higher than the ion temperature ($T_e \gg T_i$), the floating potential of the spherical particle mainly depends on the flux of energetic electrons to its surface and is always negative with respect to

† Email address for correspondence: jaiijichoudhary@gmail.com

the plasma potential. In a dusty plasma, which is an admixture of the plasma species and submicron to micron-sized solid particles, the charge on the dust grains determines their collective dynamics such as dust acoustic waves (Barkan, Merlino & D'Angelo 1995; Bandyopadhyay *et al.* 2008; Dharodi, Tiwari & Das 2014; Choudhary, Mukherjee & Bandyopadhyay 2016) and vortex motion (Law *et al.* 1998; Vaulina *et al.* 2004; Saitou & Ishihara 2013; Choudhary, Mukherjee & Bandyopadhyay 2017, 2018; Choudhary *et al.* 2020). In a dusty plasma, a dust particles are assumed to be spherical capacitors, which allows us to determine the surface potential and the net charge on it.

In recent years, the research field of dusty or complex plasmas has been of interest due to its applications in space or solar plasmas (Goertz 1984, 1989; Mendis & Rosenberg 1994), plasma processing technologies (Selwyn, Heidenreich & Haller 1991; Watanabe 1997), fusion devices (Winter 2000), colloidal solutions (Löwen *et al.* 2011), etc. For studying the collective dynamics of the dust grain medium, the charge on the dust grains has to be known. In the last more than three decades, various experimental methods have been used to obtain the dust charge in an unmagnetized dusty plasma (Wu & Miller 1990; Barkan, D'Angelo & Merlino 1994; Goree 1994; Walch, Horanyi & Robertson 1994; Khrapak *et al.* 2005). The experimentally measured dust charge values were compared with theoretically obtained values using the orbital motion limited (OML) approximation (Mott-Smith & Langmuir 1926; Allen 1992) and numerical simulations (Khrapak *et al.* 2005). The OML theory describes the charging mechanism of submicron to micron-sized particles ($r < \lambda_{De}$) in the plasma environment. Here, r is the radius of the particle and λ_{De} is the electron Debye length. For large dust grains or spherical objects ($r > \lambda_{De}$), the thin sheath theory (TS) or the modified OML theory (Willis *et al.* 2010) is suitable to understand the charging mechanism in an unmagnetized plasma.

Nowadays, magnetized dusty plasma is a popular research topic among the dusty plasma community. It is well known that the dynamics of dusty plasmas depends on the characteristics of the background plasma that can be changed in the presence of an external magnetic field. Therefore, the B-field is considered as an external parameter to control the dynamics of the dust grain medium which may allow to us study fluid dynamics, solid state phenomena, turbulence, etc. at a microscopic level (Morfill & Ivlev 2009; Bonitz, Henning & Block 2010). Since the dust charge depends on the background plasma, the estimation of the accurate charge on dust grains (magnetic or non-magnetic) is a challenge depending on the magnetization of the plasma particles. In the last few years, theoretical as well as experimental works have been carried out to estimate the charge on dust grains in the magnetized plasma. Tsytovich, Sato & Morfill (2003) performed simulations to understand the charging mechanism of micron-sized dust particles in a magnetized plasma. It has been claimed that the B-field influences the dust charging mechanism at a strong B-field when the electron gyration radius is greater than the dust radius. Lange (2016) performed a simulation of a magnetized radio-frequency (rf) plasma and observed a smaller dust surface potential (or charge) at a lower magnetic field. The simulation of Patacchini, Hutchinson & Lapenta (2007) demonstrated the decrease of the dust charge at all values of magnetic field in a collisonless plasma. A recent simulation (Kodanova *et al.* 2019) suggests that the dust charge starts to decrease after a critical value of B-field in a magnetized plasma. Yukihiro *et al.* (2009) reported a higher dust surface potential or large dust charge in a weakly magnetized plasma. Apart from analytical and numerical simulation studies, a few experiments have been performed to obtain the dust charge in a magnetized plasma. Kalita *et al.* (2015) have measured the dust charge in a weakly magnetized plasma ($B < 0.05$ T) and found the role of the B-field to be negligible on the dust charging mechanism. Tadsen, Greiner & Piel (2018) have observed a reduction of the dust charge up to 50 % for nano-sized particles at a low magnetic field ($B < 0.01$ T) in an

https://doi.org/10.1017/S0022377820001130 Published online by Cambridge University Press

rf discharge. In this work, the charge on nano-sized non-magnetic particles is determined by fitting the theoretical dispersion relation of dust-acoustic waves to the experimentally observed dispersion relation. An experimental work of Melzer *et al.* (2019) shows a reduction in the dust charge at low magnetic field ($B < 0.02$ T) and nearly constant value up to $B > 5$ T. In their work, the charge on micron-sized dust grains is extracted by a normal mode analysis of the dust cluster in the magnetized rf plasma. A similar rf discharge configuration and normal mode analysis technique were used to get the charge on micron-sized paramagnetic particles at low B-field ($B < 0.01$ T) and observed a nearly constant value of the dust charge (Puttscher & Melzer 2014). The inconsistencies in the numerically, as well as experimentally, observed values of the dust charge leave many open questions on the charging mechanism of spherical particles (magnetic and non-magnetic) in a magnetized plasma. Does the dust charge remain unchanged even though the magnetic field modifies the background plasma? How does it depend on the density of the plasma species and the background gas in the presence of a B-field? Do magnetic particles attain similar charges than non-magnetic particles? Does the surface potential of a dust grain show a size dependence in a magnetized plasma? Why does the experimentally estimated dust charge not vary according to the theoretical models?

To answer some of these questions, a better understanding of the dust charging in an rf magnetized plasma is required. It is sometimes difficult to measure a small variation in the charge of micron-sized dust grains ($r < \lambda_{De}$) while the background plasma parameters are changing in the presence of an external magnetic field. In laboratory experiments, it is easy to directly measure the surface potential of a large spherical conducting body ($r > \lambda_{De}$), which can be considered as a large dust grain in a magnetized plasma. The surface potential variation of a spherical probe (or large dust grain) in presence of an external magnetic field can provide information on a background plasma to minimize the errors in measuring the charge on micron-sized particles ($r < \lambda_{De}$) in a magnetized dusty plasma. It is well known that the charge on an individual dust particle is higher (more negative) than that of a particle in the dust grain cluster. However, the variation of the dust charge of a single dust grain and dust cluster would be similar. Sometimes the surface potential of a large dust grain also helps us to understand the interactions among the micron-sized dust grains in a magnetized plasma. Keeping this in mind, experiments are planned to measure the surface potential of magnetic and non-magnetic spherical probes (or large dust particles) in a magnetized rf discharge.

The investigations are carried out in a magnetized complex plasma device where an rf glow discharge is ignited between two electrodes, and a superconducting electromagnet is used to introduce the magnetic field. The surface potential of various sized magnetic (stainless steel (SS), SS-430, $\mu_r = 1800$) and non-magnetic (bronze, $\mu_r \sim 1$) spherical probes (or large dust grains) has been measured in the unmagnetized and magnetized plasma at various discharge conditions. At a lower magnetic field, the magnitude of the surface potential of a spherical object increases to a maximum value and then starts to decrease with an increasing of the strength of the B-field. This trend is found to be independent of the size and type of material of the spherical object. However, the charging mechanism of magnetic and non-magnetic spherical objects depends on the magnetic field. The charge or surface potential of a non-magnetic spherical probe in the plasma is found to be smaller (less negative) than that of a magnetic sphere after a threshold value of a B-field. Experimentally observed results are explained on the basis of the current collection to the surface of the object in the presence of a magnetic field.

The manuscript is organized as follows. Section 2 deals with the detailed description of the experimental set-up and the magnetized plasma production. The surface floating potential variation at various discharge conditions in unmagnetized and magnetized

https://doi.org/10.1017/S0022377820001130 Published online by Cambridge University Press

plasmas are discussed in § 3. Qualitative and quantitative explanations of the surface potential variation for magnetic and non-magnetic spheres are given in § 4. A brief summary of the work along with concluding remarks is provided in § 5.

2. Experimental set-up and diagnostics

The experimental set-up (magnetized dusty plasma device) consists of an aluminium vacuum chamber and a superconducting electromagnet, which is shown in figure 1(*a*). This device was previously used to study the dusty plasma in a strong magnetic field (Schwabe *et al.* 2011). The schematic diagram of the experimental set-up is presented in figure 1(*b*). The superconducting electromagnet has a Helmholtz coil configuration to produce a uniform magnetic field at the centre of the vacuum chamber. The superconducting magnet consists of a helium compressor, a cooling head, eight sensors for temperature measurements, and a superconducting magnet power supply (0 to 80 A). At first, the plasma chamber is evacuated below 10^{-2} Pa using a pumping system consisting of a rotary and turbo molecular pump (known as a TMP). The experiments are performed in an argon plasma and the pressure of the argon gas inside the chamber is controlled by a mass flow controller (known as an MFC) and a gate valve controller. A 13.56 MHz rf generator with matching network is used to ignite the gas discharge between a stainless steel electrode (lower) and an indium tin oxide (ITO) coated glass electrode (upper) of 6.5 cm diameter. Both electrodes are separated by 3 cm. For the comparative study, stainless steel (SS-430, $\mu_r = 1800$, magnetic) spherical probes of radius 1.0 mm, 1.25 mm and 1.7 mm and a bronze (non-magnetic, $\mu_r \sim 1$) spherical probe of radius 1.5 mm are used. Opposite radial ports are used to insert the spherical probes and the emissive probe for measuring the floating and plasma potentials. The measurements are taken in the homogeneous plasma region where the magnetic field is uniform. The spherical probes are placed in the plasma using a ceramic tube of diameter 2 mm which protrudes into the plasma by a feed-through in the chamber wall and holds the spherical probes at its end. To avoid the floating potential perturbation due to the connecting aluminium tube (it holds ceramic tube), the length of the ceramic tube is taken longer so that it only remains in contact with the plasma, as is shown in figure 1(*c*). We have made a connection to the spherical probe in such a way as to keep the connection area as small as possible compared with the total surface area. For measuring the time-averaged floating potential (V_f) of a spherical probe (or large dust grain), a high-impedance voltage divider (1200 : 1) is used. The spherical probe is connected to a high-value resistor ($R_1 = 120$ MΩ) to minimize the current flowing in the voltage divider circuit. First the voltage drop (V_2) with respect to ground due to this small current is measured across a low value resistor ($R_2 = 100$ kΩ) and then the floating potential of the spherical probe (V_f) is calculated by using the expression, $V_f = (R_1 + R_2)V_2/R_2$. In the present set of experiments, an emissive probe made of tungsten of radius 0.05 mm, placed perpendicular to the magnetic field lines, is used to measure the time-averaged plasma potential (V_p). Floating potential method technique is used to measure V_p in the absence and presence of the magnetic field (Fujita *et al.* 1980; Bradley, Thompson & Gonzalvo 2001; Balan *et al.* 2003; Sheehan *et al.* 2011; Choudhary 2017). It has been claimed in some studies that the floating potential method underestimates the plasma potential (Schrittwieser *et al.* 2005; Sheehan *et al.* 2011). In view of this, we have compared the plasma potential values obtained from the cold single Langmuir probe and the emissive probe. The floating potential method estimates the plasma potential lower by <2 V than estimated by a cold probe. This potential difference is within the error of $<15\,\%$. Thus, the floating potential method is useful to get an approximate value of plasma potential to obtain V_s.

https://doi.org/10.1017/S0022377820001130 Published online by Cambridge University Press

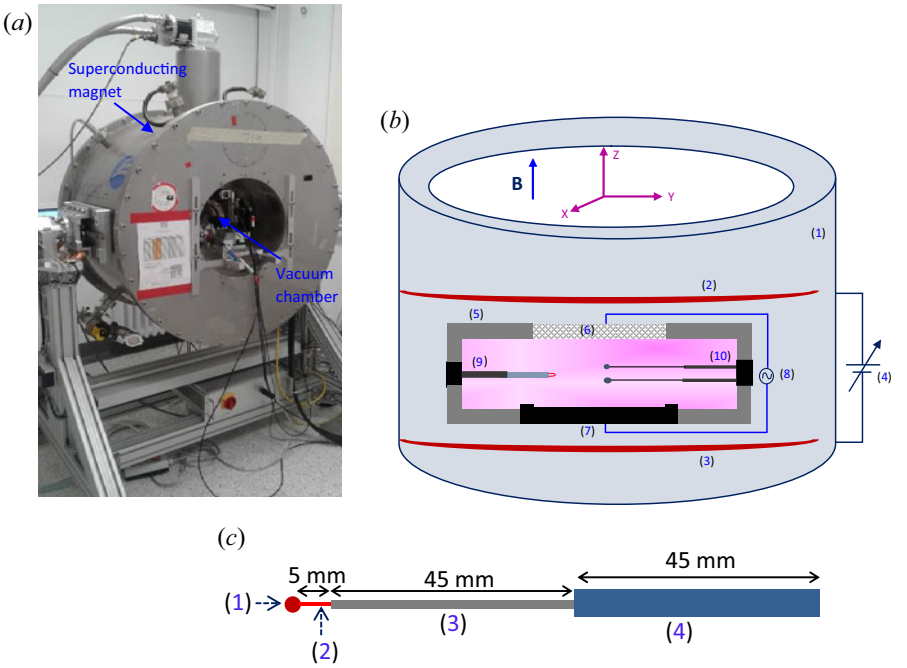

FIGURE 1. (*a*) Magnetized dusty plasma device. (*b*) Schematic diagram of the experiment set-up (1) superconducting electromagnet, (2) and (3) are superconductor coils, (4) power supply for magnet, (5) vacuum chamber, (6) upper electrode, (7) lower electrode, (8) 13.56 MHz rf generator with matching network, (9) emissive probe and (10) spherical probes. The direction of the magnetic field along the Z-direction is represented by a blue arrow. (*c*) Schematic diagram of the spherical probe (1) conducting (non-conducting) sphere, (2) connecting wire (insulation shielded), (3) ceramic tube of diameter 2 mm and (4) aluminium tube of diameter 6 mm.

3. Measurements of surface potential of spherical objects

A spherical object or dust grain immersed in a plasma attains a negative potential to balance both the electron and ion currents to its surface. This equilibrium surface potential with respect to the plasma potential (V_p) is termed as surface potential ($V_s = V_p - V_f$) of the spherical object (Chen 2003; Conde 2011). It is stated in Willis *et al.* (2010) that different analytical theories are valid for estimating the surface potential of an object in a Maxwellian plasma. The OML theory (Allen 1992) is applicable for small objects ($\rho = r/\lambda_{De} \ll 1$) and the surface potential is derived by balancing the electron and ion fluxes to the surface of an object (Willis *et al.* 2010; Beadles, Wang & Horányi 2017)

$$\exp(-\Phi) = \sqrt{\frac{T_i}{T_e}\frac{m_e}{M_i}}\left(1 - \frac{V_s}{T_i}\right), \tag{3.1}$$

where $\Phi = -V_s/T_e$, T_e and T_i are the electron and ion temperatures, m_e and M_i are the electron and ion masses, respectively. For the large spherical object ($\rho \gg 1$), the TS is applicable to obtain V_s. The surface potential for such spherical objects can be estimated by (Stangeby 2000; Willis *et al.* 2010)

$$-V_s = \frac{T_e}{2}\left[\left(2\pi\frac{m_e}{M_i}\right)\left(1 + \frac{T_i}{T_e}\right)\right] + \ln 2. \tag{3.2}$$

https://doi.org/10.1017/S0022377820001130 Published online by Cambridge University Press

In the transition region between OML and TS theory, the orbital motion (known as OM) theory estimates the surface potential. Then V_s is found to be a straight line fit on a log plot between the OML limit and TS limit (Willis *et al.* 2010; Beadles *et al.* 2017). It is clear from (3.2) and (3.3) that the floating surface potential (V_s) of a large spherical object or small dust grain has an approximately linear relation with T_e,

$$V_s = -\alpha T_e. \tag{3.3}$$

Here α is a constant varying from ∼2.5 to 4 in the transition region between the OML and TS ($0.1 < \rho < 10$) for an unmagnetized argon plasma ($T_i \ll T_e$) (Willis *et al.* 2010; Beadles *et al.* 2017). In a magnetized plasma, V_s also depends on T_e but the value of α may be lower or higher than that of an unmagnetized plasma. For finding the value of the floating surface potential, $V_s = V_p - V_f$, of a spherical conducting probe in the plasma, it is necessary to measure the plasma potential (V_p) as a reference potential. By knowing the surface potential (V_s), the charge on the surface (Q_s) of a small dust grain ($r < \lambda_{De}$) and large dust grain ($r > \lambda_{De}$) can be estimated using the different approximations (Delzanno & Tang 2015).

3.1. *Surface potential of spherical probes in unmagnetized plasma*

The present work deals with spherical probes (large dust grains) of radius larger than the electron Debye length, i.e. $r > \lambda_{De}$. Stainless steel spheres of radius 1.0 mm, 1.25 mm and 1.7 mm are used to study the size dependence of the surface potential. A pair of spherical probes of different sizes (separated by 14 mm) is placed in the plasma volume, as shown in the schematic diagram (see figure 1*b*). It should be noted that both probes are placed in the horizontal (X–Y) plane. The distance between the probes is decided after successive measurements of V_f for both spherical probes at similar discharge conditions in the presence of a B-field. These successive measurements are taken at the centre of the plasma volume whereas the simultaneous measurements on both sides of the centre are performed to keep both probes in the homogeneous plasma background. The difference between the successive and simultaneous measured values of V_f at the same discharge condition are found to be <0.3 V, which is <2–3 % of the actual value. Therefore, we neglect the shadow/potential overlapping effect of an individual sphere on each other during the simultaneous measurements of V_f for the comparative study. It is known that dust grains (μm to mm) respond only to a very low frequency external field (∼1 to 100 Hz). They do not respond to a high frequency field of an rf discharge. In view of this, it is our aim to measure the time-averaged or DC potential of the spherical probes in the rf discharge.

Figures 2(*a*) and 2(*b*) show the time-averaged V_p, V_f and V_s for different rf powers at constant pressure and for different pressures at constant power, respectively. We see a slight variation in the potentials at different discharge conditions in the absence of the magnetic field ($B = 0$ T). To see the effect of the object size on V_s at a given discharge condition ($P = 12$ W and $p = 30$ Pa), the floating potential of the stainless steel spherical probes of different sizes are measured. The variation of V_s for different sized spherical probes is depicted in figure 3. For finding the theoretical values of V_s for the given discharge conditions, the plasma density (n) and electron temperature are measured using the double probe (Johnson & Malter 1950; Nobata 1963; Choudhary 2017).

The double probe is made of two tungsten wires (or single probes) of radius 0.15 mm and length 8 mm. Both probes are separated by ∼7 mm. At $p = 30$ Pa, the plasma is moderately collisional; therefore the collisionless OML theory (Mott-Smith & Langmuir 1926; Chen 2003) of the cylindrical probe underestimates the plasma density. To measure

https://doi.org/10.1017/S0022377820001130 Published online by Cambridge University Press

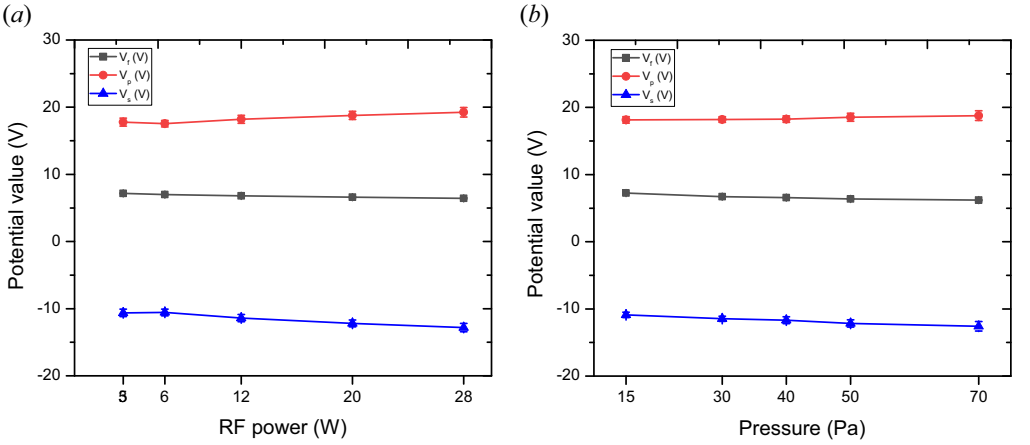

FIGURE 2. (*a*) Time-averaged floating potential (V_f), plasma potential (V_p) and surface potential (V_s) of the spherical stainless steel probe ($r = 1.7$ mm) for different input rf powers at fixed pressure, $p = 30$ Pa in an unmagnetized plasma. (*b*) The V_f, V_p and V_s of the same spherical probe for different argon pressures at fixed rf power $P = 12$ W in an unmagnetized plasma. The plotted values of V_f and V_p are averaged over few data sets at given discharge condition.

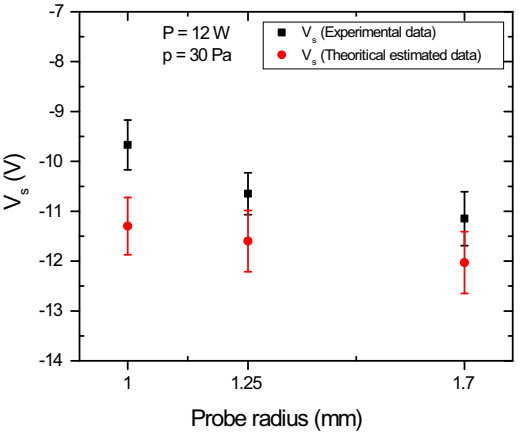

FIGURE 3. Experimental and theoretical surface potentials (V_s) of different sized stainless steel spherical probes ($r = 1$, 1.25 and 1.7 mm) at rf power, $P = 12$ W and gas pressure, $p = 30$ Pa in an unmagnetized plasma. The error in measuring the plasma potential is $<\pm 5\,\%$ and floating potential is $<\pm 2\,\%$. Both errors are included over the average values.

the approximate plasma density, the collisional model for the ion current to the cylindrical probe is used (Tichy *et al.* 1997; Kudrna & Passoth 2007). The variation of T_e and n with different rf powers is depicted in figure 4. At this discharge condition, λ_{De} is $\sim$0.3 mm, which gives $2 < \rho < 6$. The theoretically estimated values corresponding to this ρ (Willis *et al.* 2010) are plotted with experimental data (figure 3) and found to be in good agreement within the error of $\sim$10 %, which is expected due to the plasma collisionality. It confirms that the surface potential of a spherical object depends on its size in a low-temperature unmagnetized plasma ($T_e \gg T_i$).

https://doi.org/10.1017/S0022377820001130 Published online by Cambridge University Press

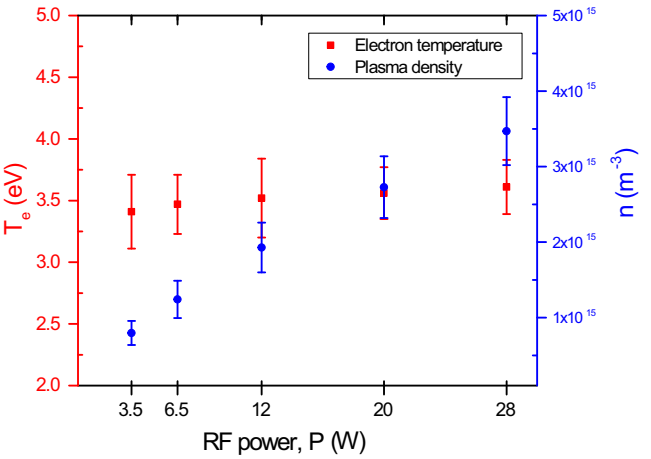

FIGURE 4. Plasma density (n) and electron temperature (T_e) at different rf powers. The measurements are carried out at fixed argon pressure, $p = 30$ Pa in unmagnetized plasma.

3.2. *Surface potential of spherical probes in magnetized plasma*

For producing the magnetized plasma, a B-field perpendicular to the plane of electrode (in the Z-direction) is applied. In figure 5 the surface potential of the SS probe of radius 1.25 mm and bronze probe of radius 1.5 mm at various strengths of the magnetic field are presented. It should be noted that the B-field is uniform in the entire plasma region at $B = 0.2$ T. The plots in figure 5(a) show the variation of V_s for different input rf powers, $P = 3.5$, 6.5 and 12 W at a fixed pressure, $p = 30$ Pa. It is clearly seen in this figure that V_s first increases (becomes more negative) at low B ($B < 0.05$ T), attains a maximum value and after that it starts to decrease (becomes less negative) at higher magnetic field strength ($B > 0.05$ T). The rate of change of V_s is observed to be different in the low B-field region ($B < 0.05$ T) and high B-field region ($B > 0.05$ T) at a given input power. It is also noticed that V_s attains its maximum value at low B-field at a lower input power ($P = 3.5$ W) and at high B-field at a higher input power ($P = 12$ W).

The variation of V_s at a given power ($P = 12$ W) and different pressures, $p = 15$, 30 and 50 Pa with the magnetic field strength is presented in figure 5(b). The rate of change of V_s is less at higher pressures for $B > 0.05$ T. It confirms the V_s dependence on the plasma collisionality. Moreover, V_s achieves its maximum value at lower B if the gas pressure is reduced. A similar trend of V_s variation is observed for the different sized magnetic spherical probes in the presence of a B-field. The variation of V_s against B for a non-magnetic sphere (bronze) is depicted in figure 5(c). The surface potential shows a similar trend to that of the magnetic sphere (figure 5b) in the presence of a B-field. However, the rate of change of V_s for the non-magnetic and magnetic sphere are different at the same discharge conditions.

3.3. *Comparison of surface potentials*

The V_s data of the magnetic probes and the non-magnetic probe are compared to see the fundamental differences in the charging mechanism in a magnetized plasma. Comparison of V_s for the magnetic and non-magnetic spheres at different B-field is depicted in figure 6. We take simultaneous measurements of the floating potential of a pair of spherical probes at a given discharge condition. At the same discharge condition, the floating potential is measured for different pairs of spherical probes with different sizes. It should be noted

https://doi.org/10.1017/S0022377820001130 Published online by Cambridge University Press

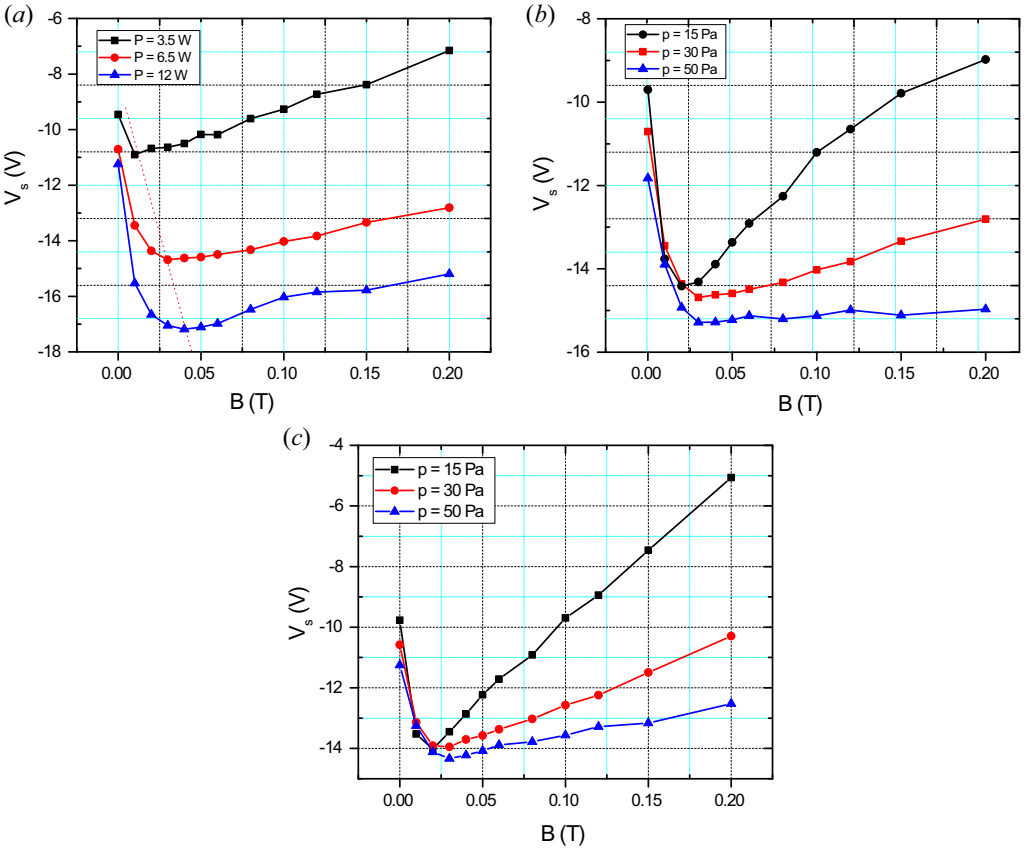

FIGURE 5. (*a*) Time–averaged surface potential (V_s) of the stainless steel spherical probe ($r =$ 1.25 mm) for different rf powers at fixed pressure, $p = 30$ Pa, in the plasma at different strengths of the magnetic field. The dotted line represents the shifting of the maxima of V_s with increasing the input rf power. (*b*) Time-averaged V_s of the stainless steel spherical probe ($r = 1.25$ mm) for different argon pressures at rf power, $P = 12$ W in magnetized plasma. (*c*) Time–averaged V_s of the bronze spherical probe ($r = 1.5$ mm) for different argon pressures at rf power, $P = 12$ W in the plasma at different strengths of magnetic field. Here, the plotted values of V_s are averaged over few data sets at given discharge condition.

that the error in V_f measurement is $<\pm 2\,\%$ and the reference potential (V_p) is common for all measurements at similar discharge conditions. This gives almost an accurate trend of the potential difference. In figure 6(*a*) the surface potential of the bronze probe has been subtracted from the magnetic ones. It is reconstructed from the V_s data for different sized ($r = 1.0$ mm, 1.25 mm and 1.7 mm) SS and bronze ($r = 1.5$ mm) probes to compare the size dependence in the presence of the *B*-field. It is clear from figure 6(*a*) that the smaller sized magnetic sphere (e.g. $r = 1$ mm) has a higher value of V_s than the non-magnetic sphere (e.g. $r = 1.5$ mm) above $B > 0.03$ T. This difference in V_s increases with increasing *B*-field. It means that equally sized magnetic and non-magnetic spherical objects or dust grains have different charges in a magnetized rf discharge. Figure 6(*b*) compares the surface potential of the different sized magnetic spheres to see the role of the *B*-field in the determination of V_s. It is seen in figure 6(*b*) that the difference in V_s for different sized magnetic probes decreases with increasing magnetic field and remains almost constant

https://doi.org/10.1017/S0022377820001130 Published online by Cambridge University Press

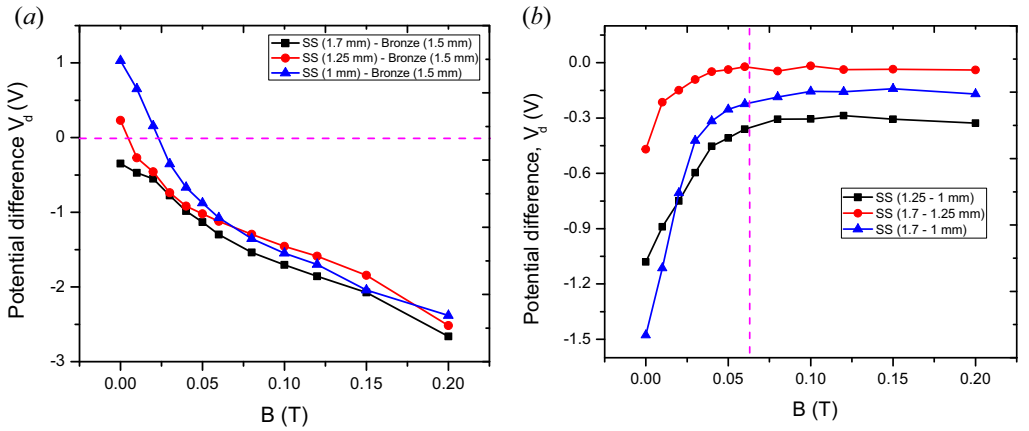

FIGURE 6. (*a*) The surface potential difference (V_d) for non-magnetic (bronze) and magnetic (SS) spherical probes at pressure, $p = 30$ Pa and rf power, $p = 12$ W in the plasma at various strengths of the magnetic field. (*b*) The difference of V_s for different sized magnetic (SS) spherical probes at pressure, $p = 30$ Pa and rf power, $P = 12$ W in magnetized plasma.

at higher B-field ($B > 0.05$ T). It shows that α remains almost constant for all sized spherical probes at higher B-field, $B > 0.05$ T. In other words, V_s has a much weaker size dependence in a magnetized rf plasma.

4. Discussion

The surface potential of a spherical probe or dust grain is determined by the electron and ion currents to its surface. In a low-temperature plasma, where $T_i \ll T_e$, the surface potential is mainly determined by T_e. Since $v_{\text{the}} \gg v_{\text{thi}}$, the surface potential is always negative with respect to the plasma potential. Here, v_{the} and v_{thi} are the electron and ion thermal velocities, respectively. In an unmagnetized rf discharge plasma (at $B = 0$ T), the surface potential of a spherical object of the radius $r > \lambda_{De}$ is estimated using the theoretical value of α in the transition region between OML and TS regions (Willis *et al.* 2010, 2012). A slight variation in T_e (see figure 4) with increasing the power and pressure demonstrates a negligible change in V_s in the unmagnetized plasma (see figure 2).

With the application of a magnetic field, the gyroradius of electrons ($r_{\text{ge}} = m_e v_{\text{the}}/eB$) and of ions ($r_{\text{gi}} = m_i v_{\text{thi}}/eB$) decreases with increasing B-field. Due to the mass differences, electrons are magnetized at lower magnetic field than ions, i.e. $r_{\text{ge}} \ll r_{\text{gi}}$. The electrons and ions are considered to be magnetized when the gyration frequency of the respective species ($\omega_{\text{ce/ci}}$) is higher than the collisional frequency ($\nu_{e-n/i-n}$), i.e. $r_{\text{ge/i}} < \lambda_{e-n/i-n}$. Here $\lambda_{e/i}$ is the collisional mean free path for the respective species. In our experiments ($p = 15$ to 50 Pa and $P = 3.5$ to 12 W), n and T_e are observed to vary between $\sim 6 \times 10^{14}$ m^{-3} and 3×10^{15} m^{-3} and 3–5 eV, respectively. The mean free path of electrons, $\lambda_{e-n} = 1/n_g \sigma_{e-n} \sim 14$–3 mm and ions, $\lambda_{i-n} = 1/n_g \sigma_{i-n} \sim 0.2$–0.08 mm. Here $\sigma_{e-n} \sim 2 \times 10^{-20}$ m^2 and $\sigma_{i-n} \sim 1 \times 10^{-18}$ m^2 are the collision cross-sections of electrons and ions with argon atoms, respectively

(Benyoucef *et al.* 2010), and n_g is the neutral gas density. The electron gyroradius varies between $r_{\text{ge}} \sim 0.5$–0.7 mm for $B = 0.01$ T at given discharge conditions. Therefore, the condition $r_{\text{ge}} < \lambda_{e-n}$ meets even below $B = 0.01$ T. With an increasing of the strength of the magnetic field ($B > 0.01$ T), r_{ge} continuously decreases and electrons are fully magnetized. Ions are assumed to be at room temperature, i.e. $T_i \sim 0.03$ eV. The ion

https://doi.org/10.1017/S0022377820001130 Published online by Cambridge University Press

gyroradius r_{gi} at $B = 0.2$ T is estimated as ∼0.5 mm, which indicates that ions get magnetized at high magnetic field, $B > 0.2$ T. It essentially means that in the range of the magnetic field ($B < 0.2$ T), only electrons are magnetized but ions are assumed to be unmagnetized. In a magnetized plasma, the currents I_e and I_i to the surface of a spherical probe are altered when the condition, $r_{ge/i} < \lambda_{De}$, is satisfied. Here $\lambda_{De} = \sqrt{\epsilon_0 k_B T_e / e^2 n_e}$ is the electron Debye length. In the present work, λ_{De} varies between ∼0.2 and 0.5 mm for the given range of plasma parameters. It shows that the electron current gets changed as a B-field is introduced. The ions do not fulfil this criteria at $B < 0.2$ T, therefore, the ion current to the surface of the spherical object is considered to be unaffected.

In an unmagnetized plasma, a constant flux of energetic electrons is lost to the chamber wall. The magnetic field confines the electrons, which definitely reduces the electrons loss to the chamber wall. Therefore, it is expected that the density of the energetic electrons would be increased as the magnetic field is introduced. To see the effect of the B-field on the electron population, the EEDF is measured using a tungsten cylindrical probe of length $l_p = 8$ mm and radius $r_p = 0.15$ mm. The probe is positioned perpendicular to the discharge axis or magnetic field lines. At discharge condition ($P = 12$ W and $p = 30$ Pa), $r_p < \lambda_{De}$, therefore, the conventional probe theory of a cylindrical probe is used to get the EEDF. It should be noted that the plasma anisotropy in the presence of the magnetic field depends on the parameter B/p and this value should be higher than 3×10^{-2} T/Pa (Behnke *et al.* 1999). Since in our set of experiments, the ratio of B/p varies from $\sim 1 \times 10^{-4}$ to 2×10^{-3} T/Pa, it does not exceed 3×10^{-2} T/Pa. Therefore, we do not expect any substantial anisotropy of the plasma or EEDF in our measurements. It should also be noted that the second derivative probe method gives a reliable EEDF in the range of the diffusion parameter (Demidov *et al.* 1999) $\Psi = r_p(\ln(\pi l_p/4r_p)/\gamma r_{ge}) < 30$ (Popov *et al.* 2012). Here, γ is constant and we assumed $\gamma \sim 4/3$ for our pressure regime. In our case, the diffusion parameter has the value $\Psi < 15$ for $B < 0.1$ T; therefore, this method is used to get the EEDF to show the increase in the energetic electron population as the B-field is turned on. The EEDF is estimated from the second derivative of the probe I-V characteristics with respect to the probe voltage (Godyak 1990; Kudrna & Passoth 2007; Popov *et al.* 2012),

$$F(E) = \frac{2\sqrt{2m_e}}{A_p e^3}\sqrt{E}\frac{\mathrm{d}^2 I_e}{\mathrm{d}V^2}, \tag{4.1}$$

where $E = \mathrm{eV} = e(V_p - V_b)$, I_e is the electron current to probe, V_b is the probe bias, V_p is the plasma potential and A_p is the area of probe. The EEDF with magnetic field at $p = 30$ Pa and $P = 12$ W is shown in figure 7(*a*). The population of the cold (or lower energy) electrons, which are reaching the probe, decreases with increasing B-field whereas the population of the energetic electrons increases at low $B < 0.05$ T (see inset image). It means that the energetic electrons can easily reach this probe surface at low B-field.

It is obvious that the average electron energy will increase due to the increase of the density of energetic electrons. It means T_e is expected to increase while the magnetic field is introduced. Since the variation in T_e affects the surface potential of a spherical object (see (3.3)), it is measured using a double or single probe at various strengths of the B-field. The inverse slope of $\ln(\mathrm{EEPF}) = \ln(F(E)/\sqrt{E})$ with respect to E (see figure 7*b*) gives T_e. It should be noted that the single probe used to obtain the EEDF is not compensated and overestimates T_e, therefore, errors concerning T_e are expected at low B-field. At higher B ($B > 0.09$ T), the secondary plasma around the probe tip during the positive bias does not give true I–V characteristics, which is also a cause of error in the T_e measurement even though it is rf compensated.

https://doi.org/10.1017/S0022377820001130 Published online by Cambridge University Press

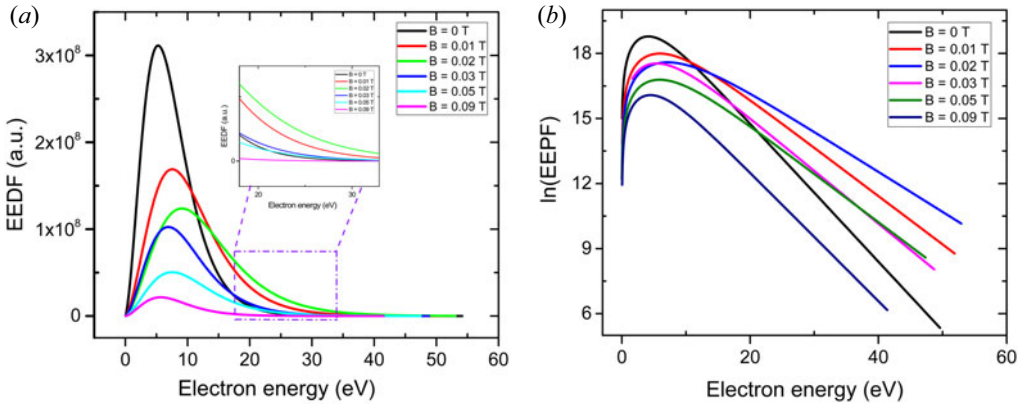

FIGURE 7. (*a*) Electron energy distribution function (EEDF) with external magnetic field at gas pressure, $p = 30$ Pa and rf power, $P = 12$ W. The inset image represents the enhancement of the energetic electron population with the application of a magnetic field. (*b*) The plots of ln(EEPF) for given EEDF at various strengths of the magnetic field.

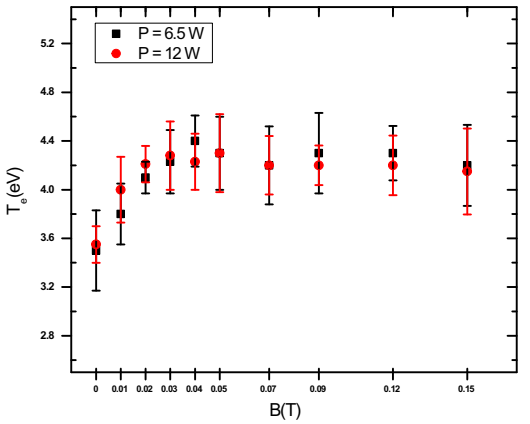

FIGURE 8. Electron temperature (T_e) variation with magnetic field at pressure, $p = 30$ Pa and rf powers, $P = 6.5$ and 12 W.

In view of this, a double probe is used to obtain the approximate value of T_e up to $B \sim 0.15$ T. The double probe theory (Johnson & Malter 1950) estimates reliable plasma parameters (n and T_e) in rf discharges if electrons obey the Maxwellian distribution, i.e. the EEDF should be Maxwellian in the presence of the B-field. In figure 7(*b*), ln(EEPF) is plotted against the electron energy E for different values of B. The ln(EEPF) against E shows the characteristics of a Maxwellian plasma (Godyak, Piejak & Alexandrovich 1993) in the experiments. Figure 8 represents the variation of the electron temperature (T_e) with magnetic field at $p = 30$ Pa and $P = 6.5$ and 12 W.

In the magnetized plasma, the net electron current I_e to the spherical probe is a sum of the electron currents to different positions on the probe (Patacchini *et al.* 2007). In the present experiments, it is difficult to estimate the electron current as a function of position (with respect to the magnetic field direction) on the spherical probe surface (Patacchini *et al.* 2007). Therefore, a simple model which considers the net electron current (I_e) in two possible directions along the B-field ($I_{e\|}$) and transverse to the B-field ($I_{e\perp}$) is used to explain the observed results qualitatively. Here $I_{e\|}$ and $I_{e\perp}$ are assumed to be the electron

https://doi.org/10.1017/S0022377820001130 Published online by Cambridge University Press

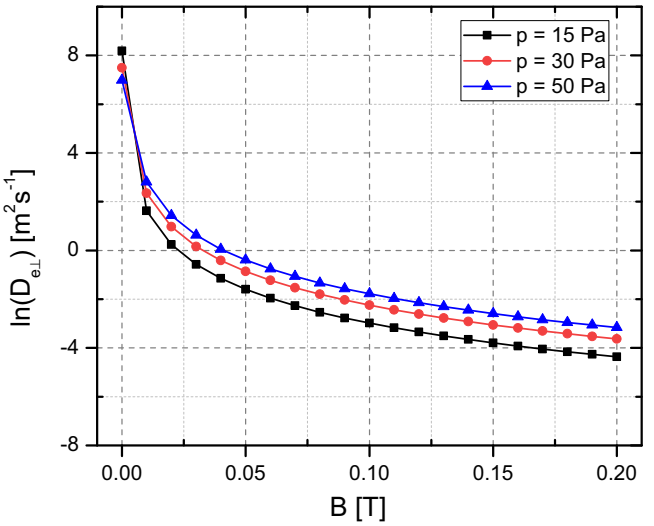

FIGURE 9. Logarithm plots of transverse diffusion coefficient ($D_{e\perp}$) for different argon pressures at various strengths of magnetic field.

current components at a given position on the spherical probe with respect to the magnetic field direction. The total electron current to the surface of a spherical probe is $I_e = I_{e\parallel} + I_{e\perp}$, which determines the floating surface potential of a probe in a magnetized plasma. It should be noted that the electron motion transverse to the B-field is much more hindered than that along the B-field in the moderately collisional plasma. In other words, $I_{e\perp}$ is reduced much more than $I_{e\parallel}$ in a magnetized plasma (Sanmartin 1970; Bohm, Burhop & Messey 1994), i.e. $D_{e\perp} < D_{e\parallel}$, where $D_{e\perp}$ and $D_{e\parallel}$ are the transverse and longitudinal diffusion coefficients, respectively.

There are two possible diffusion processes: the first one is the drain diffusion and the second one is the collisional diffusion. In drain diffusion, electrons may change their direction and cross the B-field during the motion in rf oscillating sheath field of a spherical object. In collisional diffusion, the gyrating electrons collide with background neutrals and diffuse across the B-field with a higher rate (Bohm *et al.* 1994). The drain diffusion mainly dominates over the collision diffusion in a low pressure magnetized plasma. Since the present work is performed in a moderately collisional plasma, the collisional diffusion process is considered to be more effective. For moderately collisional low-temperature magnetized plasmas, the collisional transverse diffusion coefficient is $D_{e\perp} = D_{e0}/(1 + \omega_{ce}^2\tau_e^2)$, where $D_{e0} = \lambda_{e-n}v_{the}/3$ is the diffusion coefficient in the absence of a B-field, $\omega_{ce} = eB/m_e$ is the electron cyclotron frequency and $\tau_e = \lambda_{e-n}/v_{the}$ is the electron–neutral collision time (Chen 1984; Bohm *et al.* 1994; Curreli & Chen 2014).

In a collisionless magnetized plasma, the electron motion is restricted by the magnetic field in the transverse direction. Therefore, the $D_{e\parallel}$ (or $I_{e\parallel}$) play a dominant role in the determination of the surface potential (or charge) of the dust grain in the presence of magnetic field (Patacchini *et al.* 2007). The logarithmic plots of transverse diffusion coefficient, $\ln(D_{e\perp})$, are shown in figure 9 which show a reduction in $D_{e\perp}$ after a magnetic field strength of 0.01 T. The value of $D_{e\perp}$ increases with the pressure while the magnetic field strength ($B > 0.02$ T) is kept constant, which is also illustrated in figure 9.

In the low magnetic field regime ($B < 0.05$ T), the increase in T_e (see figure 8) enhances the surface potential (more negative) of a spherical probe according to (3.3). Now, the

https://doi.org/10.1017/S0022377820001130 Published online by Cambridge University Press

probe collects a higher net current (I_e) than I_{e0}. Here, I_{e0} represents an equilibrium electron current to the spherical probe in unmagnetized plasma. This can also be understood on the basis of energetic electron population. Experimentally, the dominating role of energetic electrons in the charging process of a spherical object or dust grain in the plasma have been confirmed (Arnas, Mikikian & Doveil 1999). Since the Larmor radius of the energetic electrons ($T_e > 20$ eV) lies between 1.5 mm and 0.4 mm for $B < 0.05$ T, energetic electrons are considered to be weakly magnetized. Since $D_{e\perp}$ decreases in this B-field regime ($B < 0.05$ T), the net electron current to spherical surface should be lowered. However, the opposite behaviour (large I_e or V_s) is observed at low B-field because of the confinement of energetic electrons (or higher T_e). The higher charges on the dust grains or more negative surface potential in a weakly magnetized plasma is also observed numerically by Yukihiro *et al.* (2009). They claimed a larger absorption cross-section for electron capture on the dust surface in the presence of a magnetic field. In the present study, higher charges on a spherical probe are due to the increase of T_e for the higher magnetic field (see figure 8).

At higher B-field ($B > 0.05$ T), a lower value of the mean free path ($r_{ge} < \lambda_{e-n}$) increases the electron–neutral collision frequency, resulting in a reduction of T_e. A slight reduction in T_e at higher B is seen in figure 8. At fixed gas pressure, transverse diffusion coefficient ($D_{e\perp}$) decreases with the increasing magnetic field (see figure 9) which causes a reduction in $I_{e\perp}$. It is also observed in numerical simulations that $I_{e\parallel}$ starts to decrease with an increase of the B-field. However, this reduction in $I_{e\parallel}$ is small compared with the reduction in $I_{e\perp}$ in the magnetic field regime ($B < 0.15$ T). Therefore, it is assumed that the reduction in $I_{e\perp}$ to the spherical probe could be a possible cause of lower or less negative surface potential at high B-field ($B > 0.05$ T), which is shown in figure 5.

Since $D_{e\perp}$ (or $I_{e\perp}$) varies with $1/B^2$ at a given pressure, V_s should have a $1/B^2$ dependence. In figure 10(*a*), V_s is plotted against $1/B^2$ for different spherical probes between $B = 0.06$ T and 0.2 T. Figure 10(*a*) clearly indicates that V_s decreases linearly with $1/B^2$ between $B \sim 0.06$ T and 0.15 T for an rf power of 12 W. However, the upper B-field value shifts to a slightly lower value ($B > 0.10$ T) for the low power discharge ($P = 6.5$). Since plasma density is different in both cases ($P = 12$ W and 6.5 W) at $p = 30$ Pa, different rates of reduction of V_s with $1/B^2$ are expected. The plots of V_s against $1/B^2$ for different pressures at given power ($P = 12$ W) are shown in figure 10(*b*). We also see a linear variation of V_s with $1/B^2$ below $B < 0.12$ T and a nonlinear reduction in V_s above $B > 0.12$ T (above $p \geq 30$ Pa). For the low pressure case ($p = 15$ Pa), the nonlinear behaviour of V_s is observed at a magnetic field of >0.10 T. The different linear rates of V_s at different pressures (figure 10*b*) are expected because of different plasma backgrounds (plasma density and T_e) at a fixed input rf power and different gas pressures. In a similar plasma background, we could expect a constant linear rate of V_s with $1/B^2$ at different pressures according to the theoretical estimation as shown in figure 9. It shows that the reduction in I_e (or V_s) is mainly due to the lower value of $I_{e\perp}$ in this magnetic field regime.

At strong magnetic field strength, the contribution of $I_{e\perp}$ to I_e starts to reduce and a larger contribution comes from $I_{e\parallel}$ (Sanmartin 1970). Hence the role of $D_{e\parallel}$ (or $I_{e\parallel}$) becomes more important in the determination of the surface potential. In the present experiments, V_s does not decrease linearly with $1/B^2$ above $B > 0.12$ T (figure 10) except for the low density plasmas ($p = 30$ Pa, $P = 6.5$ W and $p = 15$ Pa, $P = 12$ W). In moderately collisional plasma, a reduction in $I_{e\parallel}$ is expected while the magnetic field increases but it could be comparable or larger than that of $I_{e\perp}$ at strong B-field (Sanmartin 1970). The nonlinear characteristics of V_s against $1/B^2$ above $B > 0.12$ T (see figure 10) is expected due to a dominant role of $I_{e\parallel}$ along with $I_{e\perp}$ for determining the surface potential. In some

https://doi.org/10.1017/S0022377820001130 Published online by Cambridge University Press

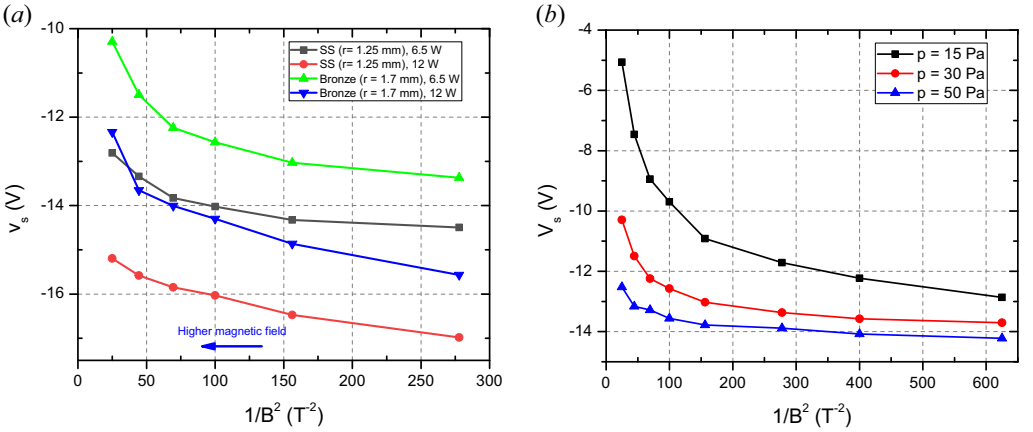

FIGURE 10. (*a*) Surface potential variation with $1/B^2$ for different spherical probes at pressure $p = 30$ Pa and rf powers, $P = 6.5$ W and 12 W. The values of $1/B^2$ are correspond to $B = 0.06$ T to 0.2 T (*b*) V_s variation against $1/B^2$ for bronze probe ($r = 1.7$ mm) at rf power 12 W and different pressures. The values of $1/B^2$ are correspond to $B = 0.04$ T to 0.2 T.

other experiments and simulations a reduction in V_s of a spherical object with increasing magnetic field has also been reported (Dote, Amemiya & Ichimiya 1964; Lange 2016; Tadsen *et al.* 2018).

It is known that the current $I_{e\perp}$ to the spherical probe decreases with increasing $\omega_{ce}\tau_e$ or decreasing $D_{e\perp}$. At given finite B-field, $D_{e\perp}$ increases with increasing electron–neutral collisions or gas pressure, which leads to an increase of $I_{e\perp}$. At finite B-field ($B > 0.01$ T), $D_{e\perp}$ has a slightly larger value at higher pressure ($p = 50$ Pa) than at lower pressure ($p = 15$ Pa), as shown in figure 9. The difference in $D_{e\perp}$ for different pressures at finite B-field is one of the possible causes for the different values of V_s in the presence of a magnetic field (figure 5*b*). The spherical surface collects more electron current at higher pressure ($p = 50$ Pa) because of the large value of $D_{e\perp}$. The lower value of $D_{e\perp}$ causes a smaller electron current to the spherical probe. Therefore, the spherical probe has a higher value (more negative) of V_s at $p = 50$ Pa than at $p = 15$ Pa (figure 5) in the magnetized plasma ($B > 0.05$ T). These results confirm the dominating role of the collisional diffusion over the drain diffusion in a moderately collisional magnetized plasma.

It should be noted that in an unmagnetized plasma ($B = 0$ T), the dust charge or surface potential decreases with an increase of the pressure due to the higher ion–neutral collision frequency (Khrapak *et al.* 2005). It is also known that collisions of plasma species with neutrals retard the motion along the magnetic field, hence reduction in $I_{e/i\|}$ is expected with increasing the gas pressure. Since ions are unmagnetized below the magnetic field of <0.2 T, the role of ions is negligible compared with the electrons in the determination of the surface potential in this given magnetic field regime ($B < 0.2$ T). Due to the smaller gyroradius of electrons (higher gyrofrequency) above $B > 0.05$ T, the electron–neutral collision frequency is found to be larger. It means that collisions lower the $I_{e\|}$ more effectively than $I_{i\|}$ in the magnetized discharge. Hence the role of ion current for determining the surface potential at different pressures ($p = 15$ to 50 Pa) is assumed to be negligible above $B > 0.05$ T. The higher negative value of V_s at higher pressure also confirms a dominant role of $I_{e\perp}$ in the reduction of the net electron current (I_e) or the surface potential in the magnetized plasma.

https://doi.org/10.1017/S0022377820001130 Published online by Cambridge University Press

The difference in V_s for magnetic (stainless steel) and non-magnetic (bronze) spherical objects (figure 6) is understood on the basis of field line distribution around a spherical body in a magnetized plasma. Since $I_{e\perp}$ decreases faster than $I_{e\parallel}$ with the magnetic field, $I_{e\perp}$ mainly responsible for the reduction in I_e (or V_s). The magnetic flux density on either side of the magnetic sphere is less than that inside of it in the presence of a magnetic field (see figure 3.7 of Fagan (2013)), which enhances $I_{e\perp}$ to the object surface due to the large value of $D_{e\perp}$ that varies with $1/B^2$. Thus, the electron current, I_e, to the magnetic sphere increases, making the surface of the spherical object more negative (higher V_s) in the presence of B-field. In the case of the non-magnetic object (copper bronze), the magnetic flux density on either side of the sphere is slightly larger than that inside of it due to the diamagnetic characteristics of copper. The B-field line density on either side of the non-magnetic sphere is expected to be higher than that around the magnetic sphere, which reduces $I_{e\perp}$ to the object surface. The lower value of the electron current (I_e) to the non-magnetic sphere makes the surface less negative. Hence a magnetic sphere has a higher value (more negative) of V_s than that of a non-magnetic sphere (see figure 6*a*) above a finite value of B-field ($B > 0.03$ T).

The qualitative description presented here provides a better understanding of the observed surface potential variation for magnetic and non-magnetic spherical probes (or large dust grains) in a magnetized rf discharge. We have provided a possible charging mechanism of magnetic and non-magnetic particles based on the reduction of electron current to spherical surface. To the best of our knowledge, at present there is no analytical or simulation work for a moderately collisional magnetized plasma to support our claim. Therefore it may be possible that another charging mechanism of magnetic and non-magnetic spherical particles plays a role in a magnetized plasma.

5. Conclusion

The surface potential of magnetic (stainless steel) and non-magnetic (bronze) spherical objects in a magnetized rf discharge at various discharge conditions is measured. A 13.56 MHz rf generator is used to produce the plasma between a transparent ITO coated glass electrode and a metal electrode. A superconducting electromagnet with Helmholtz coils configuration is used to introduce an external magnetic field. The vacuum chamber is placed at the centre of the magnet to perform the experiments in a uniform magnetic field. The surface potential of different sized magnetic spherical probes ($r = 1.0$ mm, 1.25 mm and 1.7 mm) is measured and compared with a non-magnetic spherical probe ($r = 1.5$ mm) in the plasma at different strengths of the B-field. The main findings of the experimental studies are listed below.

(i) The surface potential (V_s) of the spherical object ($r > \lambda_{De}$) depends on its size in the unmagnetized plasma.

(ii) The surface potential of a spherical object either magnetic or non-magnetic increases at the low magnetic field ($B < 0.05$ T), attains a maximum value and starts to decrease with further increasing the strength of the external magnetic field ($B > 0.05$ T). The rate of change of the surface potential in the magnetized plasma strongly depends on the gas pressure as well as the plasma parameters (n and T_e).

(iii) The surface potential of magnetic spherical objects or large dust grains is found to be higher (more negative) than that of a non-magnetic sphere at the higher magnetic field ($B > 0.04$ T).

(iv) The surface potential of the spherical objects loses its size dependence characteristics in the rf discharge with the application of an external magnetic field ($B > 0.05$ T).

https://doi.org/10.1017/S0022377820001130 Published online by Cambridge University Press

The magnetic field reduces the loss of energetic electrons to the wall and confines them in the plasma volume. The average energy of bulk plasma electrons or T_e increases due to the confinement of energetic electrons. An increase in energetic electron population or T_e at lower B ($B < 0.05$) increases the electron current to the probe surface. Hence, the surface potential increases (more negative) with B and attains its peak value between $B = 0.01$ T and 0.05 T for different discharge conditions. With an increase of the B-field ($B > 0.05$ T), the electron motion transverse to the B-field as well as along the B-field is hindered, resulting in a lower electron current to the probe surface. The reduction of the net electron current makes the spherical object less negative. Since ions are assumed to be unmagnetized for the given range of the magnetic field, the role of the magnetic field on the ion current is considered to be negligible. Thus, the electron current determines the surface potential, given by the balance of the electron and ion currents. The value of V_s depends on the magnetic field line density around a spherical object which affects the current to the surface of the object. Therefore, the surface potential is lower (or less negative) for a non-magnetic sphere than for a magnetic sphere in the magnetized plasma.

This work highlights the role of the external magnetic field as well as the types of material of the spherical objects (large dust grains) on the surface potential in a low-temperature plasma. These findings will directly help to estimate the true charges on submicron to micron-sized dust grains ($r < \lambda_{De}$) in magnetized dusty plasma experiments. It has been confirmed that electron temperature increases as the magnetic field is introduced, which definitely indicates the higher dust charges at lower magnetic field. However, many simulations and experimental works suggest either no change or less negative charge on the dust grain at low B-field. We expect the reduction in the charge of dust particles ($r < \lambda_{De}$) to be similar as for a spherical probe ($r > \lambda_{De}$) in a strong magnetic field. Interestingly, the smaller magnetic or paramagnetic dust grains may acquire a more negative charge on their surface as compared with the non-magnetic dust grains in a magnetized dusty plasma. In the future, our focus will be on the direct or indirect measurement of the charge on dust grains ($r < \lambda_{De}$) in a magnetized dusty plasma to understand the dynamics of the dust grain medium. The reported experimental work may be a motive for researchers to develop an analytical or simulation model to understand the charging mechanism of magnetic and non-magnetic spherical particles in a strongly magnetized plasma.

Acknowledgements

This work is supported by the Deutsche Forschungsgemeinschaft (DFG). The authors are grateful to F. Becker for his assistance in making spherical probes and supporting experiments. The authors are also thankful to M. Kretschmer for the experimental assistance.

Editor Edward Thomas thanks the referees for their advice in evaluating this article.

REFERENCES

ALLEN, J. E. 1992 Probe theory – the orbital motion approach. *Phys. Scr.* **45**, 497.

ARNAS, C., MIKIKIAN, M. & DOVEIL, F. 1999 High negative charge of a dust particle in a hot cathode discharge. *Phys. Rev.* E **60**, 7420–7425.

BALAN, P., SCHRITTWIESER, R., IONIȚĂ, C., CABRAL, J. A., FIGUEIREDO, H. F. C., FERNANDES, H., VARANDAS, C., ADÁMEK, J., HRON, M., STÖCKEL, J., *et al.* 2003 Emissive probe measurements of plasma potential fluctuations in the edge plasma regions of tokamaks. *Rev. Sci. Instrum.* **74**, 1583–1587.

Bandyopadhyay, P., Prasad, G., Sen, A. & Kaw, P. K. 2008 Experimental study of nonlinear dust acoustic solitary waves in a dusty plasma. *Phys. Rev. Lett*. **101**, 065006.

Barkan, A., D'Angelo, N. & Merlino, R. L. 1994 Charging of dust grains in a plasma. *Phys. Rev. Lett*. **73**, 3093–3096.

Barkan, A., Merlino, R. L. & D'Angelo, N. 1995 Laboratory observation of the dust-acoustic wave mode. *Phys. Plasmas* **2**, 3563–3565.

Beadles, R., Wang, X. & Horányi, M. 2017 Floating potential measurements in plasmas: from dust to spacecraft. *Phys. Plasmas* **24** (2), 023701.

Behnke, J. F., Passoth, E., Csambal, C., Tichý, M., Kudrna, P., Trunec, D. & Brablec, A. 1999 A study of the electron energy distribution function in the cylindrical magnetron discharge in argon and xenon. *Czech. J. Phys*. **49**, 483–498.

Benyoucef, D., Yousfi, M., Belmadani, B. & Settaouti, A. 2010 PIC MC using free path for the simulation of low-pressure RF discharge in argon. *IEEE Trans. Plasma Sci*. **38**, 902–908.

Bohm, D., Burhop, E. H. S. & Messey, H. S. W. 1994 The use of probes for plasma exploration in strong magnetic fields. In *The Characteristics of Electrical Discharges in Magnetic Fields* (ed. A. Guthrie & R. K. Wakerling), chap. 2, pp. 13–76. McGraw-Hill Book Company.

Bonitz, M., Henning, C. & Block, D 2010 Complex plasmas: a laboratory for strong correlations. *Rep. Prog. Phys*. **73**, 066501.

Bradley, J. W., Thompson, S. & Gonzalvo, Y. A. 2001 Measurement of the plasma potential in a magnetron discharge and the prediction of the electron drift speeds. *Plasma Sources Sci. Technol*. **10**, 490.

Chen, F. F. 1984 *Introduction to Plasma Physics and Controlled Fusion*. Springer.

Chen, F. F. 2003 Lecture notes on Langmuir probe diagnostics. In *Mini-Course on Plasma Diagnostics, IEEE-ICOPS meeting, Korea*.

Choudhary, M. 2017 Experimental studies on collective phenomena in dusty plasmas. PhD thesis, Homi Bhabha National Institute.

Choudhary, M., Bergert, R., Mitic, S. & Thoma, M. H. 2020 Three-dimensional dusty plasma in a strong magnetic field: observation of rotating dust tori. *Phys. Plasmas* **27** (6), 063701.

Choudhary, M., Mukherjee, S. & Bandyopadhyay, P. 2016 Propagation characteristics of dust–acoustic waves in presence of a floating cylindrical object in the DC discharge plasma. *Phys. Plasmas* **23**, 083705.

Choudhary, M., Mukherjee, S. & Bandyopadhyay, P. 2017 Experimental observation of self excited co-rotating multiple vortices in a dusty plasma with inhomogeneous plasma background. *Phys. Plasmas* **24**, 033703.

Choudhary, M., Mukherjee, S. & Bandyopadhyay, P. 2018 Collective dynamics of large aspect ratio dusty plasma in an inhomogeneous plasma background: formation of the co-rotating vortex series. *Phys. Plasmas* **25**, 023704.

Conde, L. 2011 An introduction to Langmuir probe diagnostics of plasmas. Available at: http://plasmalab.aero.upm.es/~lcl/PlasmaProbes/Probes-2010-2.pdf

Curreli, D. & Chen, F. F. 2014 Cross-field diffusion in low-temperature plasma discharges of finite length. *Plasma Sources Sci. Technol*. **23**, 064001.

Delzanno, G. L. & Tang, X.-Z. 2015 Comparison of dust charging between orbital-motion-limited theory and particle-in-cell simulations. *Phys. Plasmas* **22**, 113703.

Demidov, V. I., Ratynskaia, S. V., Armstrong, R. J. & Rypdal, K. 1999 Probe measurements of electron energy distributions in a strongly magnetized low-pressure helium plasma. *Phys. Plasmas* **6**, 350–358.

Dharodi, V. S., Tiwari, S. K. & Das, A. 2014 Visco-elastic fluid simulations of coherent structures in strongly coupled dusty plasma medium. *Phys. Plasmas* **21**, 073705.

Dote, T., Amemiya, H. & Ichimiya, T. 1964 Effect of a magnetic field upon the saturation electron current of an electrostatic probe. *Japan. J. Appl. Phys*. **3**, 789.

Fagan, M. A. 2013 Fundamental studies of heap leaching hydrology using magnetic resonance imaging. PhD thesis, Department of Chemical Engineering and Biotechnology, University of Cambridge.

Fujita, H., Nowak, S., Hoegger, B. A. & Schneider, H. 1980 Potential measurements by an emissive probe in a magnetized plasma. *Phys. Lett.* A **78**, 263–265.

GODYAK, V. A. 1990 Measuring EEDF in gas discharge plasmas. In *Plasma-Surface Interactions and Processing of Materials* (ed. O. Auciello, A. Gras-Marti, J. A. Valles-Abarca & D. L. Flamm), NATO ASI Series (Series E: Applied Sciences), vol 176. Springer.

GODYAK, V. A., PIEJAK, R. B. & ALEXANDROVICH, B. M. 1993 Probe diagnostics of non-maxwellian plasmas. *J. Appl. Phys*. **73**, 3657–3663.

GOERTZ, C. K. 1984 Formation of saturn's spokes. *Adv. Space Res*. **4**, 137–141.

GOERTZ, C. K. 1989 Dusty plasmas in the solar system. *Rev. Geophys*. **27**, 271–292.

GOREE, J. 1994 Charging of particles in a plasma. *Plasma Sources Sci. Technol*. **3**, 400–406.

JOHNSON, E. O. & MALTER, L. 1950 A floating double probe method for measurements in gas discharges. *Phys. Rev*. **80**, 58–68.

KALITA, D., KAKATI, B., SAIKIA, B. K., BANDYOPADHYAY, M. & KAUSIK, S. S. 2015 Effect of magnetic field on dust charging and corresponding probe measurement. *Phys. Plasmas* **22**, 113704.

KHRAPAK, S. A., RATYNSKAIA, S. V., ZOBNIN, A. V., USACHEV, A. D., YAROSHENKO, V. V., THOMA, M. H., KRETSCHMER, M., HÖFNER, H., MORFILL, G. E., PETROV, O. F., *et al.* 2005 Particle charge in the bulk of gas discharges. *Phys. Rev.* E **72**, 016406.

KODANOVA, S. K., BASTYKOVA, N. K., RAMAZANOV, T. S., NIGMETOVA, G. N., MAIOROV, S. A. & MOLDABEKOV, Z. A. 2019 Charging of a dust particle in a magnetized gas discharge plasma. *IEEE Trans. Plasma Sci*. **47**, 3052–3056.

KUDRNA, P. & PASSOTH, E. 2007 Langmuir probe diagnostics of a low temperature non-isothermal plasma in a weak magnetic field. *Contrib. Plasm. Phys*. **37**, 417–429.

LANGE, D. 2016 Floating surface potential of spherical dust grains in magnetized plasmas. *J. Plasma Phys*. **82**, 905820101.

LAW, D. A., STEEL, W. H., ANNARATONE, B. M. & ALLEN, J. E. 1998 Probe-induced particle circulation in a plasma crystal. *Phys. Rev. Lett*. **80**, 4189–4192.

LÖWEN, H., ROYALL, C. P., IVLEV, A. & MORFILL, G. E. 2011 Charged colloidal suspensions and their link to complex plasmas. *AIP Conf. Proc*. **1397**, 201–210.

MELZER, A., KRÜGER, H., SCHÜTT, S. & MULSOW, M. 2019 Finite dust clusters under strong magnetic fields. *Phys. Plasmas* **26**, 093702.

MENDIS, D. A. & ROSENBERG, M. 1994 Cosmic dusty plasma. *Annu. Rev. Astron. Astrophys*. **32**, 419–463.

MORFILL, G. E. & IVLEV, A. V. 2009 Complex plasmas: an interdisciplinary research field. *Rev. Mod. Phys*. **81**, 1353–1404.

MOTT-SMITH, H. M. & LANGMUIR, I. 1926 The theory of collectors in gaseous discharges. *Phys. Rev*. **28**, 727–763.

NOBATA, K. 1963 Characteristics of langmuir probe in a strong magnetic field. *Japan. J. Appl. Phys*. **2**, 719.

PATACCHINI, L., HUTCHINSON, I. H. & LAPENTA, G. 2007 Electron collection by a negatively charged sphere in a collisionless magnetoplasma. *Phys. Plasmas* **14**, 062111.

POPOV, TSV. K., IVANOVA, P., DIMITROVA, M., KOVAČIČ, J., GYERGYEK, T. & ČERČEK, M. 2012 Langmuir probe measurements of the electron energy distribution function in magnetized gas discharge plasmas. *Plasma Sources Sci. Technol*. **21**, 25004–25013.

PUTTSCHER, M. & MELZER, A. 2014 Paramagnetic dust particles in rf-plasmas with weak external magnetic fields. *New J. Phys*. **16**, 043026.

SAITOU, Y. & ISHIHARA, O. 2013 Dynamic circulation in a complex plasma. *Phys. Rev. Lett*. **111**, 185003.

SANMARTIN, J. R. 1970 Theory of a probe in a strong magnetic field. *Phys. Fluids* **13**, 103–116.

SCHRITTWIESER, R., IONITA, C., BALAN, P. C., VARANDAS, C. A. F., FIGUEIREDO, H. F. C., STOECKEL, J., ADAMEK, J., HRON, M., RYSZAWY, J., TICHY, M., *et al.* 2005 Probe methods for direct measurements of the plasma potential. *Rom. J. Phys*. **50**, 723–739.

SCHWABE, M., KONOPKA, U., BANDYOPADHYAY, P. & MORFILL, G. E. 2011 Pattern formation in a complex plasma in high magnetic fields. *Phys. Rev. Lett*. **106**, 215004.

SELWYN, G. S., HEIDENREICH, J. E. & HALLER, K. L. 1991 Rastered laser light scattering studies during plasma processing: Particle contamination trapping phenomena. *J. Vac. Sci. Technol.* A **9**, 2817–2824.

SHEEHAN, J. P., RAITSES, Y., HERSHKOWITZ, N., KAGANOVICH, I. & FISCH, N. J. 2011 A comparison of emissive probe techniques for electric potential measurements in a complex plasma. *Phys. Plasmas* **18**, 073501.

STANGEBY, P. C. 2000 *The Plasma Boundary of Magnetic Fusion Devices*. Institute of Physics.

TADSEN, B., GREINER, F. & PIEL, A. 2018 Probing a dusty magnetized plasma with self-excited dust-density waves. *Phys. Rev.* E **97**, 033203.

TICHY, M., KUDRNA, P., BEHNKE, J., CSAMBAL, C. & KLAGGE, S. 1997 Langmuir probe diagnostics for medium pressure and magnetised low-temperature plasma. *J. Phys. IV Colloque* **07** (C4), C4-397–C4-411.

TSYTOVICH, V. N., SATO, N. & MORFILL, G. E. 2003 Note on the charging and spinning of dust particles in complex plasmas in a strong magnetic field. *New J. Phys*. **5**, 43–43.

VAULINA, O. S., SAMARIAN, A. A., PETROV, O. F., JAMES, B. & MELANDSO, F. 2004 Formation of vortex dust structures in inhomogeneous gas-discharge plasmas. *Plasma Phys. Rep*. **30**, 918–936.

WALCH, B., HORANYI, M. & ROBERTSON, S. 1994 Measurement of the charging of individual dust grains in a plasma. *IEEE Trans. Plasma Sci*. **22**, 97–102.

WATANABE, Y. 1997 Dust phenomena in processing plasmas. *Plasma Phys. Control. Fusion* **39** (5A), A59–A72.

WILLIS, C. T. N., COPPINS, M., BACHARIS, M. & ALLEN, J. E. 2010 The effect of dust grain size on the floating potential of dust in a collisionless plasma. *Plasma Sources Sci. Technol*. **19**, 065022.

WILLIS, C. T. N., COPPINS, M., BACHARIS, M. & ALLEN, J. E. 2012 Floating potential of large dust grains in a collisionless flowing plasma. *Phys. Rev.* E **85**, 036403.

WINTER, J. 2000 Dust: a new challenge in nuclear fusion research? *Phys. Plasmas* **7**, 3862–3866.

WU, J. J. & MILLER, R. J. 1990 Measurements of charge on submicron particles generated in a sputtering process. *J. Appl. Phys*. **67**, 1051–1054.

YUKIHIRO, T., GAKUSHI, K., TAKATOSHI, Y. & OSAMU, I. 2009 Charging of dust particles in magnetic field. *J. Plasma Fusion Res. Ser*. **8**, 273–276.